

Article

Aging of Carbon Nanotubes Increases Their Adsorption towards Tetracycline

Xinxin Zhao ^{1,2}, Huayu Liu ^{1,2}, Zhen Yan ^{1,2} and Chao Song ^{1,2,*}

¹ Shandong Key Laboratory of Water Pollution Control and Resource Reuse, School of Environmental Science and Engineering, Shandong University, Qingdao 266237, China

² Shandong Key Laboratory of Environmental Processes and Health, School of Environmental Science and Engineering, Shandong University, Qingdao 266237, China

* Correspondence: songchao@sdu.edu.cn; Tel.: +86-532-58630936; Fax: +86-532-58630907

Abstract: Due to wide range of their applications, a large amount of carbon nanotubes (CNTs) is discharged into natural water. As an inevitable environmental fate, aging changes the physicochemical properties of carbon nanotubes, which in turn affects their interactions with other pollutants. In this study, the aging of CNTs accelerated with non-thermal plasma, and the interaction between aged CNTs and tetracycline were explored. The physicochemical properties of CNTs after aging were evaluated with specific surface area, zeta potential, FTIR, Raman, and XPS analysis. Adsorption and site energy distribution analyses were applied to explore the interaction between aged carbon nanotubes and tetracycline antibiotics. After aging, the specific surface area of carbon nanotubes decreases, defects increase, and the crystal morphology is disordered. More oxygen-containing functional groups are generated on the CNTs surface, including carbonyl, carboxyl, and hydroxyl groups. In addition, aged CNTs exhibited higher adsorption capacity for tetracycline. The results indicate that carbon nanotubes can adsorb more tetracycline after aging, which means that more antibiotics such as tetracycline may be enriched and transported on carbon nanotubes.

Keywords: carbon nanotubes; aging; adsorption; site energy distribution; non-thermal plasma



Citation: Zhao, X.; Liu, H.; Yan, Z.; Song, C. Aging of Carbon Nanotubes Increases Their Adsorption towards Tetracycline. *Water* **2022**, *14*, 2731. <https://doi.org/10.3390/w14172731>

Academic Editors: Yijing Shi and Yanyan Jia

Received: 21 July 2022

Accepted: 29 August 2022

Published: 1 September 2022

Publisher's Note: MDPI stays neutral with regard to jurisdictional claims in published maps and institutional affiliations.



Copyright: © 2022 by the authors. Licensee MDPI, Basel, Switzerland. This article is an open access article distributed under the terms and conditions of the Creative Commons Attribution (CC BY) license (<https://creativecommons.org/licenses/by/4.0/>).

1. Introduction

Carbon nanotubes (CNTs) have been mass-produced and used widely due to their excellent properties in many fields, including aerospace, construction, medical, and biotechnology [1–4]. The global CNTs production reached 1000 t/a in 2009 and keeps increasing each year [5]. However, their extensive application leads to the potential release into nature. Meanwhile, the residual CNTs in soil and sediments may also transfer to surface water and even groundwater. It has been reported that the CNTs amount was about 0.025 ng/L in some natural water and even up to 400–500 µg/L in industrial sewage [5]. It is worth noting that CNTs exhibit high affinity for many heavy metals and organic pollutants and may play an important role in the migration of these pollutants [6–8]. Moreover, the adsorption capacity of CNTs primarily depends on their surface functional groups, including physical interaction with non-polar compounds and chemical interaction with polar compounds [9]. For example, pristine CNTs surfaces show high adsorption for non-polar compounds, while surface acidic groups (phenolic, carboxylic acid, and lactic acid groups) favor the adsorption of polar compounds [10–12]. To date, the sorption, aggregation, migration, deposition, and toxicity of CNTs in the natural environment have been well explored in many studies, where CNTs were regarded as static components [13–15]. However, less attention has been paid to their chemical transformation in nature, and the subsequent effects on other pollutants.

Aging is regarded as one of the primary environmental fates of many carbon materials, such as CNTs, biochar, and graphene [16]. CNTs in nature inevitably undergo different degrees of aging from the external environment, such as chemical oxidation, ultraviolet

radiation (UV), and thermal effect [16]. In addition, reactive oxygen species (ROS), produced by biological and photochemical processes, are also important factors for CNTs aging [17–19]. In fact, aged CNTs are more according to their actual form of existence in nature. Some reactions, such as oxygen addition, hydrogen abstraction, and chain scission, occur during the aging process, and thus change the physicochemical properties of CNTs [20,21]. For instance, aging can improve the hydrophilicity of carbon nanotubes. These changes might affect the adsorption of other pollutants on CNTs, resulting in a different environmental fate [16]. However, there are few studies on the aging of CNTs and their potential effects on the adsorption for other pollutants. Thus, it is vital to evaluate the aging of CNTs and their subsequent impacts.

It is a big challenge to investigate the aging of CNTs as long periods are required for the natural process to occur. A few studies have accelerated the aging with UV irradiation [16,25]. However, CNTs in nature are also exposed to ROS, which are considered as an important factor for aging. However, there is little information regarding the joint influence of ROS and UV irradiation on the aging of CNTs. Non-thermal plasma can be triggered via air ionization and generate a variety of ROS ($\cdot\text{O}$, $\cdot\text{OH}$, and O_3 , etc.) [26]. For example, the ROS amount in water is above 720 μM after plasma treatment for 5 min, which could oxidize nanomaterials and alter their surface properties and hydrophobicity [27]. Meanwhile, physical effects including UV irradiation also take place during plasma treatment and induce chain scission, hydrogen abstraction, and oxygen addition on the surface of nanomaterials [28,29]. The combination of physical and chemical effects has been reported to effectively change the surface properties of various materials (hydrophilicity, adhesion, chemical composition, etc.) [30–32]. For example, Zhou et al. simulated various ROS oxidation and physical effects that occur naturally in the environment to explore the aging of plastics [17]. Therefore, the aging of CNTs could be well accelerated with non-thermal plasma, combining both ROS oxidation and UV irradiation, and making it more appropriate to simulating the complicated natural environment.

In this study, we investigated the aging behavior of CNTs in a simulated complex environment accelerated with non-thermal plasma. Multiwalled carbon nanotubes (MWCNTs), as model CNTs, were selected for their wide application. Tetracycline, one of most widely used antibiotics, has been detected frequently at ng/L or $\mu\text{g/L}$ in natural water [33]. It is very possible for CNTs to co-exist with tetracycline and to adsorb tetracycline, implying that the aging of CNTs might also change the environmental fate of tetracycline. Hence, tetracycline was selected as a typical emerging contaminant. This study aimed to: (i) evaluate changes in the physicochemical properties of CNTs during aging accelerated with non-thermal plasma; (ii) explore the influence of aging on the adsorption of tetracycline on CNTs. This work is expected to provide new insights into the environmental risk assessment of aged CNTs.

2. Materials and Methods

2.1. Chemicals

MWCNTs (>95% purity, 3–5 nm inner diameter, 8–15 nm outer diameter, 50 μm length) and Tetracycline hydrochloride (TC, USP grade) were bought from Aladdin Reagent Corporation (Shanghai, China). Other chemicals (reagent grade) were all obtained from Sinopharm Chemical Reagent Corporation (Shanghai, China).

2.2. Aging of CNTs with Non-Thermal Plasma

The aging of CNTs was performed in a dielectric barrier discharge plasma reactor (CTP-2000, Nanjing, China), and the details are described in the Supporting Information. In brief, CNTs (0.2 g) were first suspended in 10 mL deionized water and dispersed with ultrasound for 30 min. Then, the suspension was transferred into a glass dish on a ground electrode. The input voltage was set to 70 V. The treatment was performed for 3 h, and appropriate deionized water was added every 30 min to maintain equal volume. The aged

CNTs were collected through filtering with a 0.22 μm nylon membrane and lyophilized for further experiments.

2.3. Characterization of CNTs

The functional groups of CNTs were identified with FTIR (Nicole, Waltham, MA, USA). Briefly, dried carbon nanotubes (1 mg) were mixed with KBr powder (100 mg) and pressed into a transparent sheet. Then, FTIR spectra were measured in wavenumbers from 4000 to 800 cm^{-1} with a resolution at 2 cm^{-1} . In addition, Raman spectra were also carried out to characterize the crystal structure and electronic energy band structure of CNTs using a Raman spectrometer (Thermo, Waltham, MA, USA). The pore characteristics and surface area of CNTs were analyzed with an SSA-4300 surface area analyzer at 77 K via the adsorption–desorption curve of nitrogen. Zeta potential and particle size distribution were analyzed using dynamic light scattering with a Zeta potentiometer (Malvern Instruments, Shanghai, China).

The elemental composition of CNTs was analyzed using an XPS spectroscopy (Thermo 250XI) with a monochromatic Al K X-ray source (1486.6 eV). The reduced power of the X-ray source was 150 W with a beam spot of 500 nm. Wide scans were carried out with pass energy at 70 eV, while pass energy of 20 eV was set for narrow scans of C 1s and O 1s. The neutral C 1s signal at 284.6 eV was used to correct the surface charging effects as the reference.

2.4. Interaction of Aged CNTs with Model Pollutants

TC was selected as a model emerging contaminant to evaluate the interaction between aged CNTs and model contaminants. The details of the adsorption kinetic and isothermal experiments are provided in the Supporting Information. The concentration of TC was measured using an HPLC (LC-20AT, Shimadzu, Tokyo, Japan) with C18 column (5 μm \times 4 mm \times 250 mm) and UV detector. The mobile phase (*v/v*) was composed of 0.01 M oxalic acid (80%), acetonitrile (16%), and methanol (4%). The flow rate was at 1.0 mL/min with detection wavelength at 360 nm.

2.5. Data Analysis

The equilibrium adsorption capacity of CNTs to TC was calculated according to Equation (1):

$$q_e = \frac{(C_0 - C_e)V}{m} \quad (1)$$

where C_0 and C_e are TC concentrations in the solution at the initial and equilibrium moment; m is the mass of CNTs, and V is the solution volume; q_e is TC concentration adsorbed by CNTs when equilibrium is reached.

The pseudo-first-order kinetic and pseudo-second-order kinetic model were applied to fit the adsorption data according to Equations (2) and (3), respectively [34].

$$\ln(q_e - q_t) = \ln q_e - k_1 t \quad (2)$$

$$\frac{1}{qt} = \frac{1}{K_2 q_e^2} + \frac{1}{q_e} \quad (3)$$

where q_e and q_t are adsorption equilibrium and TC amount on the CNTs at t , respectively; t is the adsorption time; k_1 and k_2 are the adsorption rate constants, which are calculated with the pseudo-first-order and pseudo-second-order kinetic equations, respectively.

The adsorption isotherm data was fitted with two models, the Langmuir model and Freundlich model according to Equations (4) and (5) [35].

$$q_e = \frac{q_{max} k_l c_e}{1 + k_l c_e} \quad (4)$$

$$q_e = k_f c_e^{\frac{1}{n}} \quad (5)$$

where q_e and C_e are the TC concentration in CNTs and water when equilibrium is reached; q_{max} and k_f are the maximum adsorption capacity and adsorption equilibrium constant of the Langmuir model, respectively; n and k_f are the Freundlich constants, related to adsorption strength and adsorption capacity, respectively.

Adsorption distribution coefficient, k_0 , is calculated according to Equation (6):

$$k_0 = \frac{q_e}{c_e} \quad (6)$$

The standard free energy change (ΔG^0) is obtained using Equation (7):

$$\Delta G^0 = -RT \ln k_0 \quad (7)$$

The standard enthalpy change (ΔH^0) and the standard entropy change (ΔS^0) are obtained according to Equations (8) and (9), respectively:

$$\Delta G^0 = -\Delta H^0 + T\Delta S^0 \quad (8)$$

$$\ln K_0 = -\frac{\Delta H^0}{RT} + \frac{\Delta S^0}{R} \quad (9)$$

where R is universal gas constant at $8.314 \text{ J mol}^{-1} \text{ K}^{-1}$, and T is absolute temperature (K).

Site energy distribution function, $F(E^*)$, is determined with condensation approximation [36]. For the Freundlich isotherm, the approximate site energy distribution is obtained from Equations (10) and (11):

$$F(E^*) = \frac{K_f n (C_s)^n}{RT} \times \exp\left(-\frac{nE^*}{RT}\right) \quad (10)$$

$$c_e = c_s \times \exp\left(-\frac{E^*}{RT}\right) \quad (11)$$

where E^* is the difference of adsorption energy at C_e and C_s . C_s stands for the solubility of the adsorbate.

3. Results and Discussion

3.1. Changes in CNTs Due to Aging

The chemical structure of CNTs was first investigated with FTIR and Raman spectroscopy (Figure 1a,b). For FTIR analysis, only a few peaks with low intensity were observed in both pristine CNTs and aged CNTs, indicating that nonpolar bonds like C=C and C-C were the main functional groups. For pristine CNTs, the signal at 860 cm^{-1} was assigned to the symmetric stretching of C-H bonds [37]. The signals at 1567 and 1029 cm^{-1} were due to the stretching vibrations of C-O [17,38]. The existence of H and O might be due to the impurity in pristine CNTs. After plasma treatment, little change was observed, suggesting that CNTs were quite stable and nonpolar bonds were still the major structure. In addition, the peak of C-O stretching vibration shifted slightly from 1029 cm^{-1} to 1010 cm^{-1} , indicating the possible changes of C-O groups during plasma treatment. Infrared spectroscopy is vibrational spectroscopy. Usually, the energy required is very low. A signal shifts to a lower wavenumber, implying that the energy required for vibration becomes lower and the group is more unstable. This may be due to the generation of auxochrome groups such as hydroxyl and other oxygen-containing groups, resulting in changes in the structure of CNTs [39,40]. In Raman spectra, two prominent peaks at $\sim 1340 \text{ cm}^{-1}$ and $\sim 1580 \text{ cm}^{-1}$ were assigned to D band and G band, resulting from the stretching vibration of sp^3 and sp^2 carbon atoms, respectively [41]. The peaks of D-band and G-band in aged CNTs shifted from 1340 cm^{-1} to 1343 cm^{-1} , and from 1584 cm^{-1} to 1581 cm^{-1} , respectively. Meanwhile, the half-width of D-band and G-band peaks widened from 96 cm^{-1} to 103 cm^{-1} , and from 64 cm^{-1} to 73 cm^{-1} , respectively. Both changes indicated that more defects and crystal

morphology disorder occurred in aged CNTs [42]. Moreover, the ID/IG ratio increased from 1.057 to 1.124 after plasma treatment, which might result from the generation of oxygen-containing functional groups on CNTs [43].

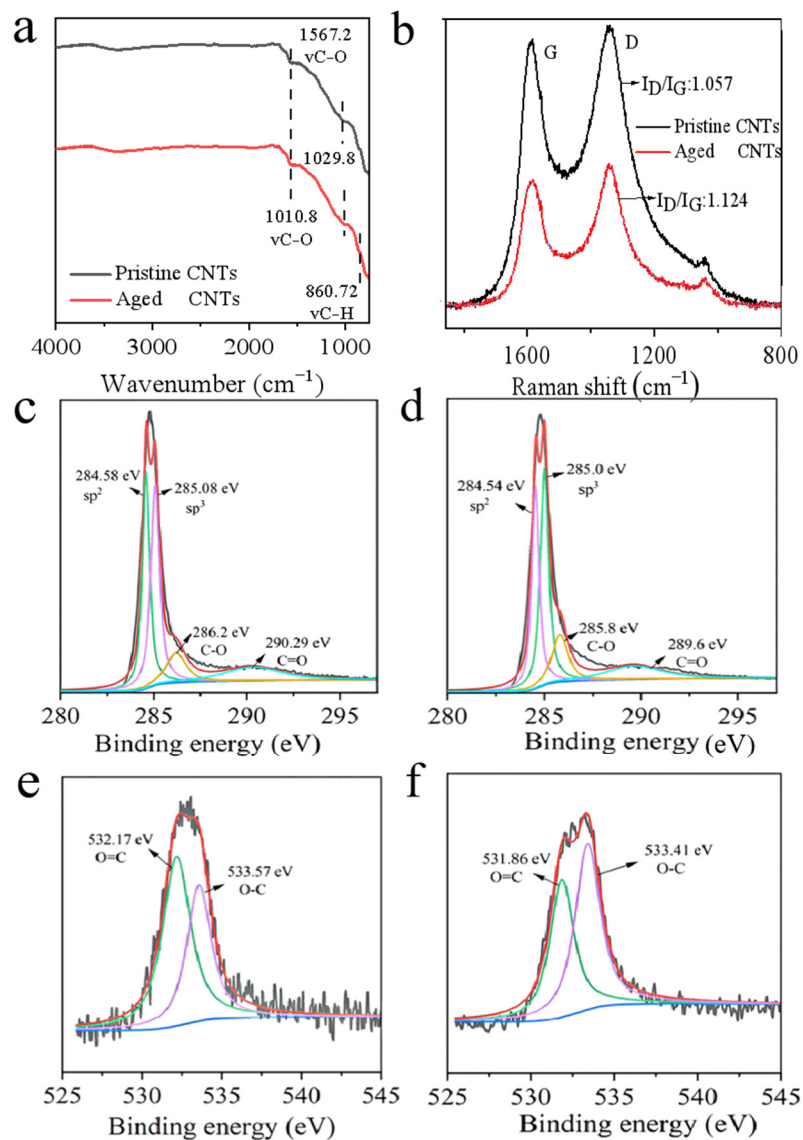


Figure 1. FTIR spectra (a) and Raman spectra (b) of pristine and aged CNTs; XPS spectra of pristine CNTs (c,e) and aged CNTs (d,f).

Furthermore, XPS spectra were recorded to explore the chemical states of pristine and aged CNTs. Two main elements, C and O, were detected with the C/O ratio at 52.19 and 25.18 in pristine and aged CNTs, respectively (Figure S3 and Table S1). These results suggested that carbon was the primary element in CNTs, and oxygen-containing groups generated during aging, which was in accordance with the FTIR and Raman results. The C 1s signal was resolved into four peaks (Figure 1), where the peaks at ~284 eV, ~285 eV, ~286 eV, and ~290 eV were associated with sp²-hybridized, sp³-hybridized, C-O, and C=O, respectively (Table 1) [44]. Meanwhile, the O1s peaks at ~532 eV and ~533.57 eV were assigned to O=C and O-C, respectively [45]. Compared to pristine CNTs, the relative amount of C-O and C=O increased from 28.5% to 30.9%, implying the generation of oxygen-containing groups like carboxylic and carbonyl groups. These results confirmed the oxidation of CNTs by generating oxygen-containing groups during the aging process. Generally, these generating groups exhibit strong hydrophilic properties and thus could

enhance the hydrophilicity of CNTs, suggesting that aged CNTs might exhibit different affinity to other pollutants [46].

Table 1. Results of deconvolution analysis of C1s and O1s spectra of the pristine and aged CNTs.

	C1s				O1s	
	sp2	sp3	C-O	C=O	O=C	O-C
Pristine CNTs						
Position (eV)	284.58	285.08	286.20	290.29	532.17	533.58
Percentage	34.2%	37.3%	12.1%	16.4%	58.9%	41.1%
Aged CNTs						
Position (eV)	284.54	285.00	285.80	289.64	531.86	533.41
Percentage	31.6%	37.4%	15.5%	15.5%	44.4%	55.6%

The pore volume, specific surface area, and surface charge were also considered as key factors that affect the adsorption of CNTs on many pollutants [4]. There was no apparent difference in total pore volume (Table 2). Mean pore size increased slightly after aging, which might improve the diffusion of adsorbate and thus enhance the adsorption. These results were also in accordance with adsorption isotherms analysis [47]. Moreover, specific surface area decreased from 81.78 to 76.42 m²/g, implying that plasma might partly sinter the surface of CNTs, collapse the crystal structure, and increase the crystal shape disorder [13]. This could increase surface defects and active sites on aged CNTs, leading to more reaction between TC and CNTs [47]. These results were consistent with the Raman analysis. As shown in Figure 2, zeta potential values of both pristine and aged CNTs reduced with the increasing pH, and the points of zero charge values (pH_{pzc}) were estimated at ~6.1 and ~4.4, respectively. Moreover, aged CNTs exhibited more negative surface charge and less positive charge at the same pH, resulting from more oxygen-containing groups on the surface [48]. Aged CNTs became more stable and dispersive in neutral water (pH = 7) with decreasing zeta potentials from −12.8 to −15.6 eV. In conclusion, lower specific surface area and higher electronegativity were detected on aged CNTs, which might affect the adsorption of other pollutants on CNTs [49].

Table 2. Specific surface area and particle size distribution of pristine and aged CNTs.

	SSA ^a (m ² /g)	TPV ^b (cm ³ /g)	MPR ^c (nm)
Pristine CNTs	81.78	0.266	6.51
Aged CNTs	76.41	0.267	6.99

Note: ^a SSA, specific surface area; ^b TPV, the total pore volume; ^c MPR, mean pore size.

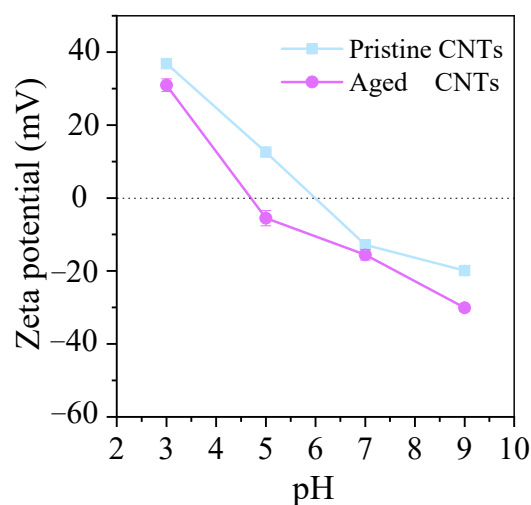


Figure 2. The zeta potential of pristine and aged CNTs.

3.2. Adsorption of TC on CNTs

CNTs can work as an excellent adsorbent for many pollutants due to their high affinity and adsorption capacity [50]. In this study, the physicochemical properties of CNTs were obviously changed during the aging process, which might directly disturb the adsorption of other pollutants on CNTs and further disturb the migration of these pollutants [51]. Tetracycline (TC), a broad-spectrum antibiotic detected frequently in aquatic environments, was selected as a model emerging contaminant to explore the adsorption behavior of aged CNTs. As shown in Figure 3a, the adsorption rates of aged CNTs were significantly slower in the initial adsorption stage than those of pristine CNTs. When equilibrium was reached, the adsorption of TC at 10 mg/L and 20 mg/L was almost the same on both pristine and aged CNTs. For high initial TC concentration (50 mg/L), aged CNTs adsorbed a little less TC at 1400 min, when the adsorption was not equilibrium due to high initial TC concentration. Furthermore, adsorption data was fitted using the pseudo-first-order and pseudo-second-order kinetic equations. The pseudo-second-order kinetic equation was a better for the adsorption of TC on both pristine and aged CNTs with similar $q_{e\text{ cal}}$ values to $q_{e\text{ exp}}$ at higher R^2 values (Table S2), implying that chemical adsorption might play the primary role [52]. The adsorption rate constants k_2 of aged CNTs were obviously lower than those of pristine CNTs, suggesting lower affinity of aged CNTs to TC. These results could explain why the adsorption of TC was significantly slower on aged CNTs in the initial adsorption stage than that on pristine CNTs. However, the similar q_e of pristine and aged CNTs were observed at equilibrium point, suggesting that lower affinity might not decrease the adsorption capacity of aged CNTs.

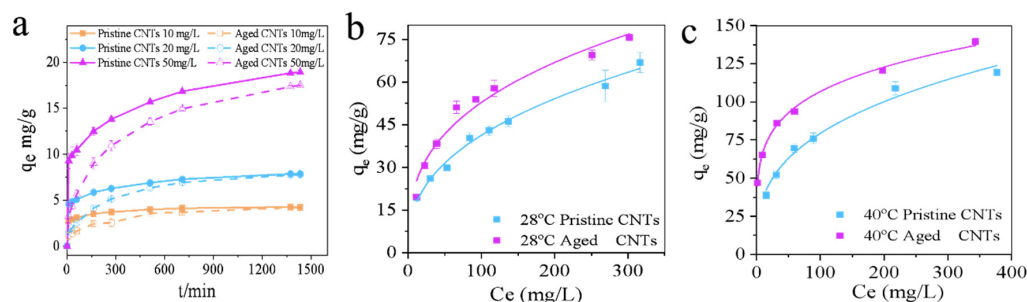


Figure 3. (a) The adsorption kinetic curve of TC on pristine and aged CNTs; Adsorption isotherms fitted with the Freundlich model of TC at 28 °C (b) and 40 °C (c).

Adsorption isotherm experiments were designed to further explore the adsorption of TC on aged CNTs. Figure 3 shows that all isotherms were non-linear. In addition, the Freundlich model was much better than the Langmuir model in describing the adsorption data with higher R^2 (Table S3). Hence, subsequent discussion was based on the adsorption parameters from the results fitted with the Freundlich model. Moreover, it is obvious that the curves of aged carbon nanotubes are above those of pristine CNTs at both 28 °C and 40 °C, suggesting that the adsorption capacity of aged CNTs is higher than that of pristine CNTs. Generally, the Freundlich isotherm model is appropriate to the adsorption on heterogeneous surfaces with varied affinities, which supposes that adsorption sites with strong affinity are first occupied and then the strength of binding weakens with increasing degree of sites occupation [36]. In this study, various oxygen-containing groups were generated on the CNTs surface during aging, and TC could adsorb on both carbon skeleton and oxygen-containing groups with varied affinities. In addition, these oxygen-containing groups also provided more sites for TC adsorption, and thus enhanced the adsorption of TC on aged CNTs. In addition, the values of q_e at 40 °C were much higher than those at 28 °C for both pristine and aged CNTs, implying that the TC adsorption on CNTs might be endothermic, and high temperature is beneficial to enhancing the adsorption.

3.3. Site Energy Distribution Analysis

The site energy distribution was calculated to explore the energetic characteristics of the interactions between CNTs and TC. E^* decreased with the increasing q_e for both pristine and aged CNTs (Figure 4a), indicating the existence of limited high-energy sites and the unevenness of site energy distribution [36]. These results were also in accordance with the adsorption isotherm analysis, which was better fitted with the Freundlich model, as heterogeneous adsorption. In addition, E^* values for aged CNTs were higher than those for pristine CNTs, which was also consistent with the order of K_f (Table S3).

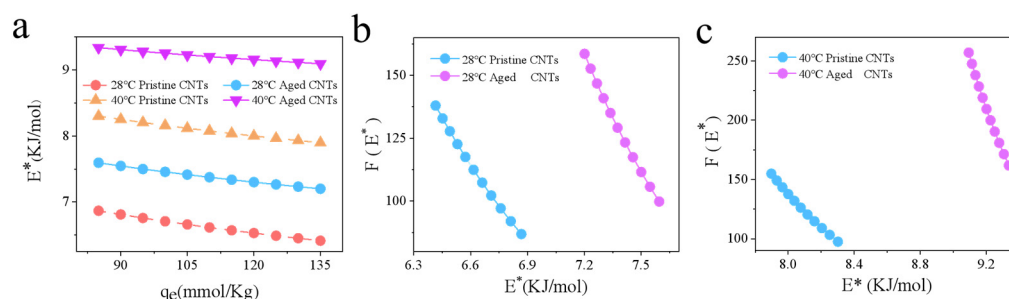


Figure 4. E^* of TC adsorption on CNTs (a); $F(E^*)$ of TC adsorption on CNTs at 28 °C (b) and 40 °C (c).

Figure 4b,c describes the site energy distribution curves for TC adsorption on pristine and aged CNTs. Obviously, all the curves exhibited similar shapes. $F(E^*)$ decreased sharply with increasing E^* , implying that there are a few high-energy adsorption sites on both pristine and aged CNTs, and TC would occupy these high-energy sites first. In addition, relative lower $F(E^*)$ suggested that the contributions of high-energy sites (>8 kJ/mol) were limited to the overall adsorption of TC. In a certain range of E^* , the area below the $F(E^*)$ curves can be regarded as the adsorption capacity and the number of available adsorption sites [35,36]. At a fixed value of E^* , $F(E^*)$ was in the order of 313.15 K $>$ 301.15 K and aged CNTs $>$ pristine CNTs for TC. These results indicated that the adsorption sites of TC increased with increasing temperature, and that aged CNTs exhibited larger adsorption capacity and more adsorption sites than pristine CNTs, which was consistent with the adsorption isotherm analysis.

3.4. Thermodynamic Analysis

Temperature is a vital factor that influences adsorption via changing the viscosity of the aqueous solution and the brown motion of adsorbate molecules [36]. In this study, adsorption of TC on CNTs improved with increasing temperature (Figure 3b,c), and the average adsorption energy (E^*) for TC is in the order of 313.15 K $>$ 301.15 K (Figure 4), confirming that the TC adsorption on CNTs is endothermic, and high temperature is positive for their adsorption [53]. Therefore, thermodynamic parameters were calculated to further explore TC adsorption on both pristine and aged CNTs [54]. As shown in Figure 5, standard free energy change (ΔG^0) values of aged CNTs were more negative than those of pristine CNTs, indicating that TC adsorption on aged CNTs was more spontaneous. Standard enthalpy (ΔH^0) values for TC were positive within the tested loadings, indicating that the TC adsorption on CNTs was endothermic. Besides, ΔH^0 increased with the increasing TC loadings, implying that TC adsorption became more endothermic. Moreover, standard entropy (ΔS^0) values of TC adsorption on both pristine and aged CNTs were positive, implying that randomness at solid–liquid interface was raised during the adsorption. Moreover, ΔS^0 values of aged CNTs increased more with the increasing loadings. These results further confirmed the conclusions of adsorption kinetics and the adsorption isotherms analysis.

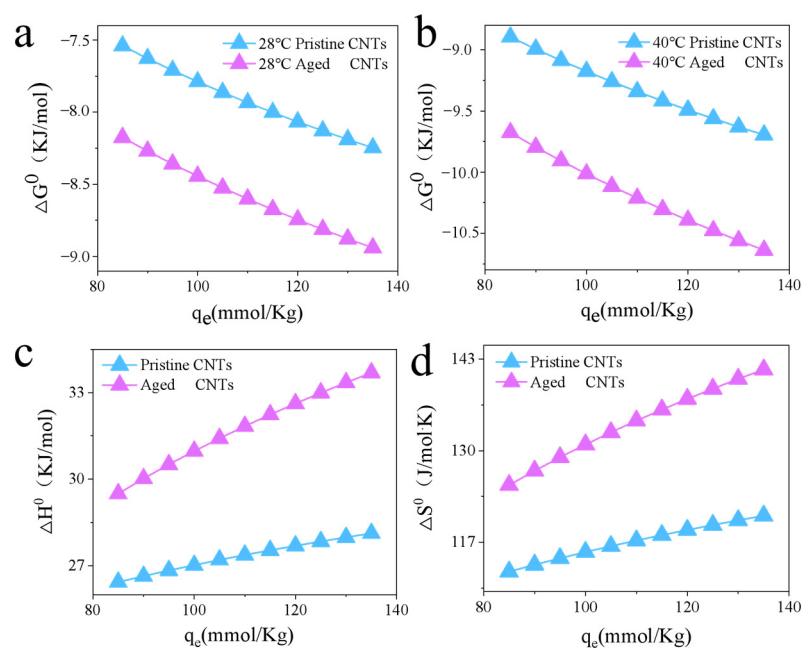


Figure 5. ΔG^0 (a,b), ΔH^0 (c) and ΔS^0 (d) of TC adsorption on pristine and aged CNTs.

3.5. Adsorption Mechanism

Adsorption is considered as an accumulation of adsorbate molecules from liquid phase to the adsorbent surfaces. For porous solids like CNTs, the adsorption process can be composed of three steps: (1) out-diffusion, when adsorbate molecules transfer through the liquid film to the outer surface of the adsorbent; (2) inner diffusion, when adsorbate molecules transfer from the exterior surface to the internal capillaries or pores of the adsorbent; (3) adsorbate molecules attach to the active sites on the internal and external surfaces of the adsorbent. The third step occurred rapidly, and thus it is not regarded as a rate-limiting step. In general, adsorption rate is limited by out-diffusion, inner diffusion, or both [55,56]. Meanwhile, the properties of both the adsorbate and adsorbent directly affect the adsorption [36]. In this study, aged CNTs exhibited higher adsorption capacity to TC but with a lower adsorption rate in the initial adsorption stage. These results were well explained by the changes in CNTs due to aging. Firstly, aged CNTs showed lower specific surface area and higher mean pore size (Table 2) with more defects and crystal morphology disorder (Figure 1). The specific surface area is also vital for physical adsorption, and it also occurs rapidly in the initial adsorption stage [57]. Lower specific surface area might be the main reason why the initial adsorption rate of TC on aged CNTs was lower than that of pristine CNTs. Besides, the porous structure of CNTs is mainly mesoporous (2–50 nm), so TC molecules are mainly adsorbed on the material surface between layers, and most TC molecules are adsorbed on the pore surface of mesoporous structure [58]. Therefore, the higher mean pore size could improve the diffusion of TC in CNTs in the subsequent adsorption stage. Secondly, more oxygen-containing groups were identified on aged CNTs surface, including carbonyl and hydroxyl groups (Figure 1). Less entanglement and more fragments of CNTs were also observed in SEM images after aging (Figure S2). Carbon nanotubes always contain many defects in structure, such as pentagonal or twist defects, heptagonal defects, and lattice defects (dangling bonds, atomic vacancies, dislocations, and interstitials) at the end caps. Defect and functional groups on aged CNTs tend to act as preferred reaction sites due to severe deformation, promoting the reaction of the chemisorption process [20]. During plasma treatment, ROS first attack the defect sites and then the edge sites, leading to the generation of oxygen-containing groups on the surfaces. There are also many polar functional groups on the TC molecule, which could interact with the oxygen-containing groups on aged CNTs via hydrogen bonding [59]. Therefore, TC could adsorb on both carbon skeleton and oxygen-containing groups of aged

CNTs, and these oxygen-containing groups provided more adsorption sites, leading to higher adsorption of aged CNTs to TC. Electrostatic interaction is also considered as an important force for adsorption. TC is an amphoteric molecule, containing three protonated groups: dimethylamino, phenolic deketone, and tricarbonyl methane group [60]. In this study, aged CNTs exhibited more negative surface charge than pristine CNTs in neutral water (pH = 7) (Figure 2). However, TC exists mainly as a zwitterion at pH = 7, and thus electrostatic interaction might play a minor role in TC adsorption on CNTs in neutral water. In addition, pristine CNTs are unstable in aqueous solution and tend to aggregate, which greatly weakens their adsorption capacity. On the other hand, aged CNTs exhibited higher hydrophilicity with better dispersity, which also promoted the adsorption of TC.

In this study, we found that the adsorption of CNTs to TC is closely related to their aging. After aging, the specific surface area of CNTs decreases. More oxygen-containing groups are formed on the surface. In addition, the adsorption rate of TC is relatively slow at the beginning, but the adsorption amount is always higher than that of pristine CNTs. Previous studies have well explored the adsorption mechanism of TC on pristine CNTs: TC molecules attach tightly on CNTs surfaces due to the roles of protonated amino group and enone structures of TC, which can interact strongly with the polarized electron-rich graphene structures of CNTs via cation- π bonding and π - π electron donor-acceptor (EDA) interactions [61–63]. On the other hand, this could not well explain the adsorption of TC on aged CNTs. In this study, the specific surface area and surface groups of aged CNTs play more important roles in TC adsorption. The reduction of specific surface area resulted in a slow initial adsorption rate, while the generation of defects and oxygen-containing functional groups provided more active sites, improved the hydrophilicity, and facilitated the formation of hydrogen bonds. Moreover, the improved dispersity increases the number of available adsorption sites, thereby facilitating TC adsorption. In addition, the TC adsorption on CNTs was endothermic, and aged CNTs exhibited larger adsorption capacity and more adsorption sites than pristine CNTs.

4. Conclusions

This study investigated the aging of CNTs and explored tetracycline adsorption on aged CNTs. Plasma can comprehensively accelerate the aging of CNTs in nature. After aging, the specific surface area of CNTs decreased with more defects and crystal morphology disorder, leading to slower adsorption rate in the initial adsorption stage. More oxygen-containing functional groups were formed on the surface of aged CNTs, including carboxyl, carbonyl, and hydroxyl groups, which provide more adsorption sites for TC. Both enhancement in dispersity and hydrophilicity promoted the adsorption of TC on CNTs. Therefore, aged CNTs exhibited higher adsorption capacity to TC but with a lower adsorption rate in the initial adsorption stage. Moreover, TC adsorption on CNTs is endothermic, implying that high temperature is positive for their adsorption. As an inevitable environmental fate, aging can change the physicochemical properties of CNTs and thus affect their interaction with other pollutants. This study provides new insight for further exploration of the aging of nanomaterials in nature. Meanwhile, CNTs can adsorb more tetracycline after aging, implying that more antibiotics like tetracycline would be enriched and transported on CNTs during the aging process, increasing the threat to the ecosystem and human health.

Supplementary Materials: The following supporting information can be downloaded at: <https://www.mdpi.com/article/10.3390/w14172731/s1>, Figure S1: Schematic diagram of plasma treatment of CNTs; Figure S2: SEM characterization of pristine CNTs (a, b) and aged CNTs (c, d); Figure S3: XPS spectra of pristine and aged CNTs; Figure S4: Adsorption isotherms fitted with Langmuir model of TC:(a)at 28 °C; (b)at 40 °C; Table S1: The chemical composition of the pristine and aged CNTs; Table S2: Kinetic parameters for the adsorption of tetracycline on the pristine and aged CNTs; Table S3: Isotherm parameters for tetracycline adsorbed by pristine and aged CNTs.

Author Contributions: Conceptualization, X.Z., H.L. and C.S.; methodology, C.S. and Z.Y.; Validation, C.S. and X.Z.; formal analysis, X.Z. and H.L.; investigation, X.Z. and H.L.; writing—original draft preparation, X.Z. and C.S.; writing—review and editing, C.S. and Z.Y. All authors have read and agreed to the published version of the manuscript.

Funding: This research was supported by the National Natural Science Foundation of China (U20A20146) and the Young Scholars Program of Shandong University.

Acknowledgments: The authors wish to thank Feifei Liu for the support on site energy distribution analysis.

Conflicts of Interest: The authors declare no conflict of interest.

References

1. Petersen, E.J.; Zhang, L.; Mattison, N.T.; O'Carroll, D.M.; Whelton, A.J.; Uddin, N.; Nguyen, T.; Huang, Q.; Henry, T.B.; Holbrook, R.D.; et al. Potential release pathways, environmental fate, and ecological risks of carbon nanotubes. *Environ. Sci. Technol.* **2011**, *45*, 9837–9856. [[CrossRef](#)] [[PubMed](#)]
2. Yang, K.; Lou, Z.; Fu, R.; Zhou, J.; Xu, J.; Baig, S.A.; Xu, X. Multiwalled carbon nanotubes incorporated with or without amino groups for aqueous Pb(II) removal: Comparison and mechanism study. *J. Mol. Liq.* **2018**, *260*, 149–158. [[CrossRef](#)]
3. Kabbani, M.A.; Tiwary, C.S.; Autreto, P.A.S.; Brunetto, G.; Som, A.; Krishnadas, K.R.; Ozden, S.; Hackenberg, K.P.; Gong, Y.; Galvao, D.S.; et al. Ambient solid-state mechano-chemical reactions between functionalized carbon nanotubes. *Nat. Commun.* **2015**, *6*, 7291. [[CrossRef](#)]
4. Wang, X.; Liu, X.; Han, H. Evaluation of antibacterial effects of carbon nanomaterials against copper-resistant *Ralstonia solanacearum*. *Colloids Surf. B Biointerfaces* **2013**, *103*, 136–142. [[CrossRef](#)]
5. Gottschalk, F.; Sonderer, T.; Scholz, R.W.; Nowack, B. Modeled environmental concentrations of engineered nanomaterials (TiO₂, ZnO, Ag, CNT, Fullerenes) for different regions. *Environ. Sci. Technol.* **2009**, *43*, 9216–9222. [[CrossRef](#)] [[PubMed](#)]
6. Sajid, M.; Asif, M.; Baig, N.; Kabeer, M.; Ihsanullah, I.; Mohammad, A.W. Carbon nanotubes-based adsorbents: Properties, functionalization, interaction mechanisms, and applications in water purification. *J. Water Process Eng.* **2022**, *47*, 102815. [[CrossRef](#)]
7. Baby, R.; Saifullah, B.; Hussein, M.Z. Carbon nanomaterials for the treatment of heavy metal-contaminated water and environmental remediation. *Nanoscale Res. Lett.* **2019**, *14*, 341. [[CrossRef](#)]
8. Chen, C.L.; Hu, J.; Xu, D.; Tan, X.L.; Meng, Y.D.; Wang, X.K. Surface complexation modeling of Sr(II) and Eu(III) adsorption onto oxidized multiwall carbon nanotubes. *J. Colloid Interface Sci.* **2008**, *323*, 33–41. [[CrossRef](#)]
9. Ong, Y.T.; Ahmad, A.L.; Zein, S.H.S.; Tan, S.H. A review on carbon nanotubes in an environmental protection and green engineering perspective. *Braz. J. Chem. Eng.* **2010**, *27*, 227–242. [[CrossRef](#)]
10. Tang, Y.; Zhang, S.; Su, Y.; Wu, D.; Zhao, Y.; Xie, B. Removal of microplastics from aqueous solutions by magnetic carbon nanotubes. *Chem. Eng. J.* **2021**, *406*, 126804. [[CrossRef](#)]
11. Tian, Y.; Gao, B.; Morales, V.L.; Wu, L.; Wang, Y.; Munoz-Carpena, R.; Cao, C.; Huang, Q.; Yang, L. Methods of using carbon nanotubes as filter media to remove aqueous heavy metals. *Chem. Eng. J.* **2012**, *210*, 557–563. [[CrossRef](#)]
12. Premarathna, K.S.D.; Rajapaksha, A.U.; Sarkar, B.; Kwon, E.E.; Bhatnagar, A.; Ok, Y.S.; Vithanage, M. Biochar-based engineered composites for sorptive decontamination of water: A review. *Chem. Eng. J.* **2019**, *372*, 536–550. [[CrossRef](#)]
13. Chen, W.; Duan, L.; Zhu, D. Adsorption of polar and nonpolar organic chemicals to carbon nanotubes. *Environ. Sci. Technol.* **2007**, *41*, 8295–8300. [[CrossRef](#)] [[PubMed](#)]
14. Hong, Y.; Shi, W.; Wang, H.; Ma, D.; Ren, Y.; Wang, Y.; Li, Q.; Gao, B. Mechanisms of *Escherichia coli* inactivation during solar-driven photothermal disinfection. *Environ. Sci. Nano* **2022**, *9*, 1000–1010. [[CrossRef](#)]
15. Jackson, P.; Jacobsen, N.R.; Baun, A.; Birkedal, R.; Kuhnel, D.; Jensen, K.A.; Vogel, U.; Wallin, H. Bioaccumulation and ecotoxicity of carbon nanotubes. *Chem. Cent. J.* **2013**, *7*, 154. [[CrossRef](#)]
16. Peng, X.; Jia, J.; Gong, X.; Luan, Z.; Fan, B. Aqueous stability of oxidized carbon nanotubes and the precipitation by salts. *J. Hazard. Mater.* **2009**, *165*, 1239–1242. [[CrossRef](#)]
17. Zhou, L.; Wang, T.; Qu, G.; Jia, H.; Zhu, L. Probing the aging processes and mechanisms of microplastic under simulated multiple actions generated by discharge plasma. *J. Hazard. Mater.* **2020**, *398*, 122956. [[CrossRef](#)]
18. Rathore, V.; Nema, S.K. Optimization of process parameters to generate plasma activated water and study of physicochemical properties of plasma activated solutions at optimum condition. *J. Appl. Phys.* **2021**, *129*, 084901. [[CrossRef](#)]
19. Chae, S.R.; Hunt, D.E.; Ikuma, K.; Yang, S.; Cho, J.; Gunsch, C.K.; Liu, J.; Wiesner, M.R. Aging of fullerene C-60 nanoparticle suspensions in the presence of microbes. *Water Res.* **2014**, *65*, 282–289. [[CrossRef](#)]
20. Srivastava, D.; Brenner, D.W.; Schall, J.D.; Ausman, K.D.; Yu, M.F.; Ruoff, R.S. Predictions of enhanced chemical reactivity at regions of local conformational strain on carbon nanotubes: Kinky chemistry. *J. Phys. Chem. B* **1999**, *103*, 4330–4337. [[CrossRef](#)]
21. Ye, B.; Kim, S.-I.; Lee, M.; Ezazi, M.; Kim, H.-D.; Kwon, G.; Lee, D.H. Synthesis of oxygen functionalized carbon nanotubes and their application for selective catalytic reduction of NO_(x) with NH₃. *RSC Adv.* **2020**, *10*, 16700–16708. [[CrossRef](#)] [[PubMed](#)]
22. Yang, J.C.E.; Zhu, M.P.; Dionysiou, D.D.; Yuan, B.; Fu, M.L. Interplay of bicarbonate and the oxygen-containing groups of carbon nanotubes dominated the metal-free activation of peroxymonosulfate. *Chem. Cent. J.* **2022**, *430*, 133102. [[CrossRef](#)]

23. Demina, T.S.; Piskarev, M.S.; Shpichka, A.I.; Gilman, A.B.; Timashev, P.S. Wettability and aging of polylactide films as a function of AC-discharge plasma treatment conditions. *J. Phys. Conf. Ser.* **2020**, *1492*, 012001. [[CrossRef](#)]
24. Khan, F.S.A.; Mubarak, N.M.; Khalid, M.; Tan, Y.H.; Abdullah, E.C.; Rahman, M.E.; Karri, R.R. A comprehensive review on micropollutants removal using carbon nanotubes-based adsorbents and membranes. *J. Environ. Chem. Eng.* **2021**, *9*, 106647. [[CrossRef](#)]
25. Panessa-Warren, B.J.; Maye, M.M.; Warren, J.B.; Crosson, K.M. Single walled carbon nanotube reactivity and cytotoxicity following extended aqueous exposure. *Environ. Pollut.* **2009**, *157*, 1140–1151. [[CrossRef](#)]
26. Xu, H.; Fang, C.; Shao, C.; Li, L.; Huang, Q. Study of the synergistic effect of singlet oxygen with other plasma-generated ROS in fungi inactivation during water disinfection. *Sci. Total Environ.* **2022**, *838*, 156576. [[CrossRef](#)] [[PubMed](#)]
27. Liu, P.; Qian, L.; Wang, H.; Zhan, X.; Lu, K.; Gu, C.; Gao, S. New insights into the aging behavior of microplastics accelerated by advanced oxidation processes. *Environ. Sci. Technol.* **2019**, *53*, 3579–3588. [[CrossRef](#)]
28. Guo, D.; Liu, Y.; Ji, H.; Wang, C.C.; Chen, B.; Shen, C.; Li, F.; Wang, Y.; Lu, P.; Liu, W. Silicate-enhanced heterogeneous flow-through electro-fenton system using iron oxides under nanoconfinement. *Environ. Sci. Technol.* **2021**, *55*, 4045–4053. [[CrossRef](#)]
29. Song, Y.K.; Hong, S.H.; Jang, M.; Han, G.M.; Jung, S.W.; Shim, W.J. Combined effects of UV exposure duration and mechanical abrasion on microplastic fragmentation by polymer type. *Environ. Sci. Technol.* **2018**, *52*, 3831–3832. [[CrossRef](#)]
30. Lukic, K.; Vukusic, T.; Tomasevic, M.; Curko, N.; Gracin, L.; Ganic, K.K. The impact of high voltage electrical discharge plasma on the chromatic characteristics and phenolic composition of red and white wines. *Innov. Food. Sci. Emerg.* **2019**, *53*, 70–77. [[CrossRef](#)]
31. Cao, S.; Zhang, Y.; He, N.; Wang, J.; Chen, H.; Jiang, F. Metal-free 2D/2D heterojunction of covalent triazine-based frameworks/graphitic carbon nitride with enhanced interfacial charge separation for highly efficient photocatalytic elimination of antibiotic pollutants. *J. Hazard. Mater.* **2020**, *391*, 122204. [[CrossRef](#)] [[PubMed](#)]
32. Guo, Q.; Wang, Y.; Zhang, H.; Qu, G.; Wang, T.; Sun, Q.; Liang, D. Alleviation of adverse effects of drought stress on wheat seed germination using atmospheric dielectric barrier discharge plasma treatment. *Sci. Rep.* **2017**, *7*, 16680. [[CrossRef](#)] [[PubMed](#)]
33. Lopez-Penalver, J.J.; Sanchez-Polo, M.; Gomez-Pacheco, C.V.; Rivera-Utrilla, J. Photodegradation of tetracyclines in aqueous solution by using UV and UV/H₂O₂ oxidation processes. *J. Chem. Technol. Biotechnol.* **2010**, *85*, 1325–1333. [[CrossRef](#)]
34. Van Son, T.; Huu Hao, N.; Guo, W.; Ton-That, C.; Li, J.; Li, J.; Liu, Y. Removal of antibiotics (sulfamethazine, tetracycline and chloramphenicol) from aqueous solution by raw and nitrogen plasma modified steel shavings. *Sci. Total Environ.* **2017**, *601*, 845–856.
35. Liu, F.F.; Zhao, J.; Wang, S.G.; Xing, B. Adsorption of sulfonamides on reduced graphene oxides as affected by pH and dissolved organic matter. *Environ. Pollut.* **2016**, *210*, 85–93. [[CrossRef](#)] [[PubMed](#)]
36. Liu, F.F.; Fan, J.L.; Wang, S.G.; Ma, G.H. Adsorption of natural organic matter analogues by multi-walled carbon nanotubes: Comparison with powdered activated carbon. *Chem. Eng. J.* **2013**, *219*, 450–458. [[CrossRef](#)]
37. Li, Z.; Hu, X.; Qin, L.; Yin, D. Evaluating the effect of different modified microplastics on the availability of polycyclic aromatic hydrocarbons. *Water. Res.* **2020**, *170*, 115290. [[CrossRef](#)]
38. Xia, P.F.; Li, Q.; Tan, L.R.; Sun, X.F.; Song, C.; Wang, S.G. Extracellular polymeric substances protect *Escherichia coli* from organic solvents. *RSC Adv.* **2016**, *6*, 59438–59444. [[CrossRef](#)]
39. Kumar, S.; Sharma, P.; Sharma, V. Redshift in absorption edge of Cd_{1-x}CoxS nanofilms. *IEEE Trans. Nanotechnol.* **2014**, *13*, 343–348. [[CrossRef](#)]
40. Gopi, R.; Ramanathan, N.; Sundararajan, K. Blue-shift of the C-H stretching vibration in CHF₃-H₂O complex: Matrix isolation infrared spectroscopy and ab initio computations. *Chem. Phys.* **2016**, *476*, 36–45. [[CrossRef](#)]
41. Liu, X.; Xu, F.; Zhang, K.; Wei, B.; Gao, Z.; Qiu, Y. Characterization of enhanced interfacial bonding between epoxy and plasma functionalized carbon nanotube films. *Compos. Sci. Technol.* **2017**, *145*, 114–121. [[CrossRef](#)]
42. Cunha, R.; Paupitz, R.; Yoon, K.; Van Duin, A.C.T.; Elías, A.L.; Carozo, V.; Dasgupta, A.; Fujisawa, K.; Lopez, N.P.; Araujo, P.T.; et al. Raman spectroscopy revealing noble gas adsorption on single-walled carbon nanotube bundles. *Carbon* **2018**, *127*, 312–319. [[CrossRef](#)]
43. Nylander, A.; Hansson, J.; Nilsson, T.; Ye, L.; Fu, Y.; Liu, J. Degradation of carbon nanotube array thermal interface materials through thermal aging: Effects of bonding, array height, and catalyst oxidation. *ACS. Appl. Mater. Interfaces* **2021**, *13*, 30992–31000. [[CrossRef](#)]
44. Gomez, S.; Rendtorff, N.M.; Aglietti, E.F.; Sakka, Y.; Suarez, G. Surface modification of multiwall carbon nanotubes by sulfonitric treatment. *Appl. Surf. Sci.* **2016**, *379*, 264–269. [[CrossRef](#)]
45. Song, C.; Sun, X.F.; Xing, S.F.; Xia, P.F.; Shi, Y.-J.; Wang, S.G. Characterization of the interactions between tetracycline antibiotics and microbial extracellular polymeric substances with spectroscopic approaches. *Environ. Sci. Pollut. Res.* **2014**, *21*, 1786–1795. [[CrossRef](#)]
46. Gao, Y.; Wang, Q.; Ji, G.; Li, A. Degradation of antibiotic pollutants by persulfate activated with various carbon materials. *Chem. Eng. J.* **2022**, *429*, 132387. [[CrossRef](#)]
47. Kumar, P.S.; Korving, L.; Keesman, K.J.; van Loosdrecht, M.C.M.; Witkamp, G.-J. Effect of pore size distribution and particle size of porous metal oxides on phosphate adsorption capacity and kinetics. *Chem. Eng. J.* **2019**, *358*, 160–169. [[CrossRef](#)]

48. Sun, Z.; Nicolosi, V.; Rickard, D.; Bergin, S.D.; Aherne, D.; Coleman, J.N. Quantitative evaluation of surfactant-stabilized single-walled carbon nanotubes: Dispersion quality and its correlation with zeta potential. *J. Phys. Chem. C* **2008**, *112*, 10692–10699. [[CrossRef](#)]
49. Liu, C.; Wang, W.; Zhu, L.; Cui, F.; Xie, C.; Chen, X.; Li, N. High-performance nanofiltration membrane with structurally controlled PES substrate containing electrically aligned CNTs. *J. Membr. Sci.* **2020**, *605*, 118104. [[CrossRef](#)]
50. Zhang, D.; Pan, B.; Zhang, H.; Ning, P.; Xing, B. Contribution of different sulfamethoxazole species to their overall adsorption on functionalized carbon nanotubes. *Environ. Sci. Technol.* **2010**, *44*, 3806–3811. [[CrossRef](#)]
51. Pourfayaz, F.; Ahmadi-Avval, P.; Tarverdi, H.; Sadegh, M.; Maleki, A.; Ahmadi, M.H. A study of effects of different surface modifications of MWCNTs on their adsorption capacity of benzene and toluene. *Iran. J. Chem. Eng.* **2017**, *36*, 107–114.
52. Yu, Q.; Zhang, R.Q.; Deng, S.B.; Huang, J.; Yu, G. Sorption of perfluorooctane sulfonate and perfluorooctanoate on activated carbons and resin: Kinetic and isotherm study. *Water Res.* **2009**, *43*, 1150–1158. [[CrossRef](#)] [[PubMed](#)]
53. Jin, Q.; Yang, Y.; Dong, X.; Fang, J. Site energy distribution analysis of Cu (II) adsorption on sediments and residues by sequential extraction method. *Environ. Pollut.* **2016**, *208*, 450–457. [[CrossRef](#)] [[PubMed](#)]
54. Wang, Z.Y.; Yu, X.D.; Pan, B.; Xing, B.S. Norfloxacin sorption and its thermodynamics on surface-modified carbon nanotubes. *Environ. Sci. Technol.* **2010**, *44*, 978–984. [[CrossRef](#)]
55. Yu, F.; Wu, Y.; Li, X.; Ma, J. Kinetic and thermodynamic studies of toluene, ethylbenzene, and m-Xylene adsorption from aqueous solutions onto KOH-activated multiwalled carbon nanotubes. *J. Agric. Food Chem.* **2012**, *60*, 12245–12253. [[CrossRef](#)]
56. Ma, J.; Yu, F.; Zhou, L.; Jin, L.; Yang, M.; Luan, J.; Tang, Y.; Fan, H.; Yuan, Z.; Chen, J. Enhanced adsorptive removal of methyl orange and methylene blue from aqueous solution by alkali-activated multiwalled carbon nanotubes. *ACS Appl. Mater. Interfaces* **2012**, *4*, 5749–5760. [[CrossRef](#)]
57. Dou, S.; Ke, X.X.; Shao, Z.D.; Zhong, L.B.; Zhao, Q.B.; Zheng, Y.M. Fish scale-based biochar with defined pore size and ultrahigh specific surface area for highly efficient adsorption of ciprofloxacin. *Chemosphere* **2022**, *287*, 131962. [[CrossRef](#)]
58. Zhang, Y.; Li, Y.; Xu, W.; Cui, M.; Wang, M.; Chen, B.; Sun, Y.; Chen, K.; Li, L.; Du, Q.; et al. Filtration and adsorption of tetracycline in aqueous solution by copper alginate-carbon nanotubes membrane which has the muscle-skeleton structure. *Chem. Eng. Res. Des.* **2022**, *183*, 424–438. [[CrossRef](#)]
59. Huo, S.; Song, X.; Zhao, Y.; Ni, W.; Wang, H.; Li, K. Insight into the significant contribution of intrinsic carbon defects for the high-performance capacitive desalination of brackish water. *J. Mater. Chem. A* **2020**, *8*, 19927–19937. [[CrossRef](#)]
60. Zhao, B.; Zhang, J. Tetracycline degradation by peroxydisulfate activated by waste pulp/paper mill sludge biochars derived at different pyrolysis temperature. *Water* **2022**, *14*, 1583. [[CrossRef](#)]
61. Yu, F.; Ma, J.; Han, S. Adsorption of tetracycline from aqueous solutions onto multi-walled carbon nanotubes with different oxygen contents. *Sci. Rep.* **2014**, *4*, 5326. [[CrossRef](#)] [[PubMed](#)]
62. Ji, L.; Chen, W.; Bi, J.; Zheng, S.; Xu, Z.; Zhu, D.; Alvarez, P.J. Adsorption of tetracycline on single-walled and multi-walled carbon nanotubes as affected by aqueous solution chemistry. *Environ. Toxicol. Chem.* **2010**, *29*, 2713–2719. [[CrossRef](#)] [[PubMed](#)]
63. Ji, L.; Chen, W.; Duan, L.; Zhu, D. Mechanisms for strong adsorption of tetracycline to carbon nanotubes: A comparative study using activated carbon and graphite as adsorbents. *Environ. Sci. Technol.* **2009**, *43*, 2322–2327. [[CrossRef](#)] [[PubMed](#)]